Supporting Information

A Multifunctional Layered $Ti_3C_2T_x/VS_2$ Composite Sulfur Host for Promoting the Conversion of Lithium Polysulfides in Lithium-Sulfur Batteries

Guisheng Deng,[a] Wen Xi,[a] Junpu Zhang,[a] Youfang Zhang,[b] Rui Wang,[a] * Yansheng Gong,[a] Beibei He,[a] Huanwen Wang,[a] Jun Jin[a] *

[a]*Faculty of Materials Science and Chemistry, China University of Geosciences, Wuhan 430074, China;*

[b]*Hubei Key Laboratory of Polymer Materials, Ministry of Education Key Laboratory for Green Preparation and Application of Functional Materials, School of Materials Science and Engineering, Hubei University, Wuhan 430062, China.*

**Corresponding author. E-mail address: jinjun@cug.edu.cn; wangrui@cug.edu.cn*

1. Material characterizations

The morphologies and structures of the synthesized composites are characterized using a scanning electron microscope (SEM, Hitachi SU-3500, Japan) and transmission electron microscope (TEM, FEI Talos F200S). The X-ray diffraction (XRD) patterns of the samples are obtained using a D8-FOCUS (Bruker AXS, Panalytical) instrument with Cu Kα radiation (1.5418 Å) at 40 kV and 40 mA. The specific surface areas and pore size distributions are tested on Micrometrics equipment at nitrogen adsorption-desorption measurements (ASAP-2460). The chemical states of $Ti_3C_2T_x/VS_2$, $Ti_3C_2T_x$, and VS_2 are investigated by X-ray photoelectron spectroscopy (XPS, Thermo Scientific K-Alpha).

2. Electrochemical characterizations

2.1 Preparation and testing of cathodes

The prepared material is ground and mixed with sulfur powder in a ratio of 3:7, then hydrothermally treated at 155 °C for 12 hours under argon atmosphere to obtain the $Ti_3C_2T_x/VS_2/S$ composite. The resulting sulfur composite material (70 wt%) and carbon nanotube (CNT) solution (30 wt%) are mixed with DI water to form a slurry, which is evenly coated onto aluminum foil. The coated foil is dried at 60 °C for 12 hours with sulfur mass loading of 0.8~0.9 mg cm^{-1}. The Li-S batteries are assembled in an argon-filled glove box in CR2032 button cells using 1.0 M LiTFSI in1,3-dioxolane (DOL) /1,2-dimethoxyethane (DME) (1:1 vol%) with 2% $LiNO_3$ as electrolyte (0.03 mL).

2.2 Preparation of 3D-printed electrodes

The printing slurry is prepared as described above and loaded into a 3 mL syringe. The syringe is connected to a tri-axis MUSASHI dispenser (SM200SX-3A-SS-01-MU-STK) for printing grid-shaped electrodes on the cathode shells at a pressure of 0.25 MPa and a printing speed of 1 mm s^{-1}. Afterward, the printed electrodes are placed in a freezer overnight and freeze-dried to obtain the 3D-printed cathodes.

2.3 Polysulfides adsorption test

For the electrolyte preparation, 0.075 mmol of Li_2S and 0.375 mmol of sulfur powders are dissolved in 7.5 mL of DOL and 7.5 mL of DME at 70 °C with stirring until completely dissolved. 15 mg of $Ti_3C_2T_x/VS_2$ (or $Ti_3C_2T_x$, VS_2) powder is added to 3 mL of the above solution, and the color change of the solution is recorded. Besides, the diluted supernatant is analyzed using a UV-vis spectrophotometer.

2.4 Linear scanning voltammetry (LSV) experiments

5 mg of active material is dispersed in 5 mL of ethanol under sonication. Then, 0.04 mL of mixture solution is doped on the carbon paper (1×1 cm^2) and then dried. A three-electrode test is conducted using an Ag/AgCl reference electrode and a platinum foil counter electrode in a 0.1 M Li_2S methanol solution as the electrolyte. The measurement is carried out at a scan rate of 5 mV s^{-1} using an electrochemical workstation (CHI660E) within a voltage window of -0.8 to 0 V.

2.5 Assembly and testing of symmetrical cells

The tested materials and CNT solution are mixed into a slurry at a mass ratio of

7:3, coated on aluminum foil, and dried at 60 °C for 12 hours. The symmetrical cells are assembled in an argon-filled glove box using test materials as both the working electrode and counter electrode, while the electrolyte consists of 0.06 mL of 0.2 M Li_2S_6 solution. The CV curves of the symmetric units are measured at scan rates of 2, 4, 6, 8, and 10 mV s^{-1}, with a voltage range of -1 to 1 V.

2.6 Li_2S nucleation and dissolution test

To study the kinetics of solid-liquid transformation of LiPSs, a 0.2 M Li_2S_8 solution is prepared using tetramethylene glycol dimethyl ether as the solvent, with the addition of 1 M LiTFSI. A symmetrical battery is assembled using $Ti_3C_2T_x/VS_2$/S as working electrode, PP film as separator, and lithium metal as counter electrode, respectively. 0.02 mL of normal electrolyte and 0.02 mL of prepared Li_2S_8 solution are added drop by drop. The battery is initially discharged at a constant current of 0.112 mA until the voltage reaches 2.07 V, followed by a constant voltage discharge at 2.02 V until the current dropped below 0.001 mA.

To examine the rate of dissolution conversion of Li_2S to LiPSs, the same cell configuration is employed. The cell is discharged to 1.7 V at a constant current of 0.112 mA and then charged at a constant voltage of 2.4 V until the current reaches 0.01 mA.

Table S1. Percentage nucleation and $activation$ time of Li_2S for $Ti_3C_2T_x/VS_2/S$, $Ti_3C_2T_x/S$, and VS_2/S.

Parameters	$Ti_3C_2T_x/VS_2/S$	$Ti_3C_2T_x/S$	VS_2/S
Percentage nucleation time of Li_2S	26.9%	28.0%	28.0%
Percentage activation time of Li_2S	1.2%	1.3%	1.8%

Table S2. Li^+ diffusion coefficients of $Ti_3C_2T_x/VS_2/S$, $Ti_3C_2T_x/S$, and VS_2/S.

Parameters	$Ti_3C_2T_x/VS_2/S$	$Ti_3C_2T_x/S$	VS_2/S
D_{Li}^{+} at peak A ($cm^2\ s^{-1}$)	1.26×10^{-8}	3.97×10^{-9}	5.93×10^{-9}
D_{Li}^{+} at peak B ($cm^2\ s^{-1}$)	2.27×10^{-9}	1.71×10^{-9}	1.93×10^{-9}
D_{Li}^{+} at peak C ($cm^2\ s^{-1}$)	5.04×10^{-9}	3.85×10^{-9}	4.68×10^{-9}

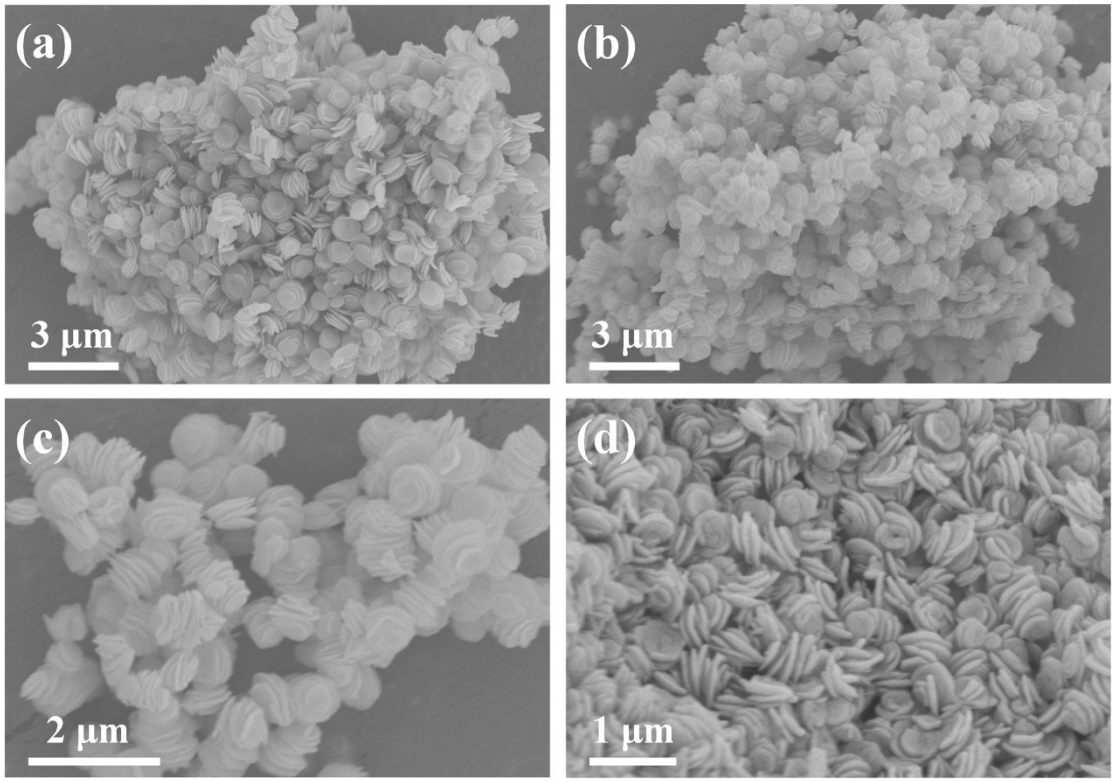

Figure S1. SEM images of VS_2 nanosheets with different magnifications.

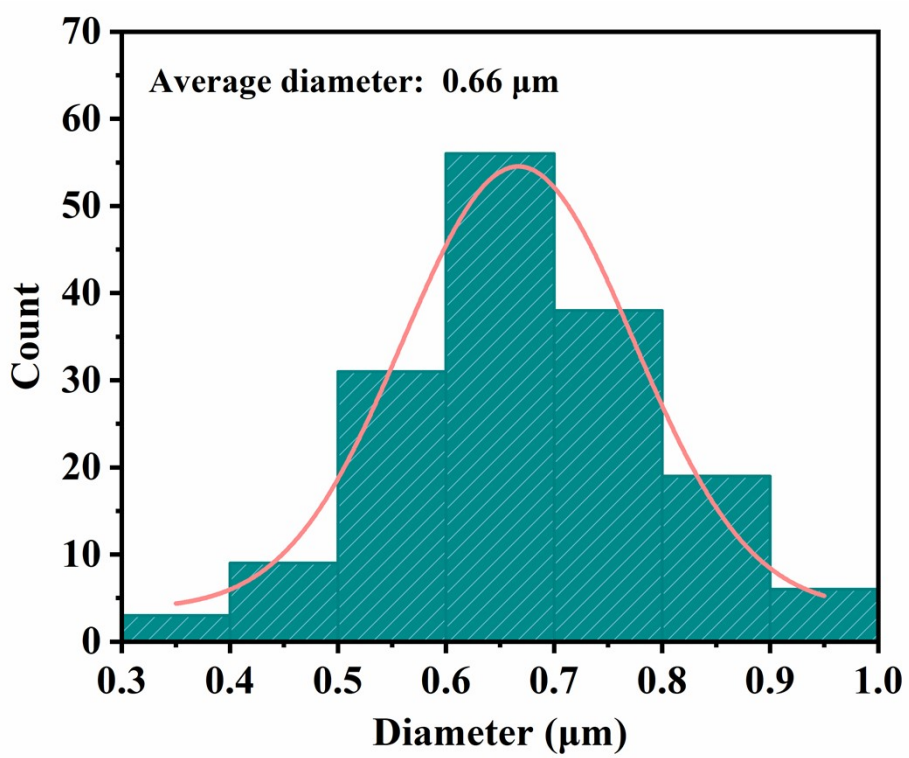

Figure S2. Statistical plot of diameter distribution of VS_2 nanosheets.

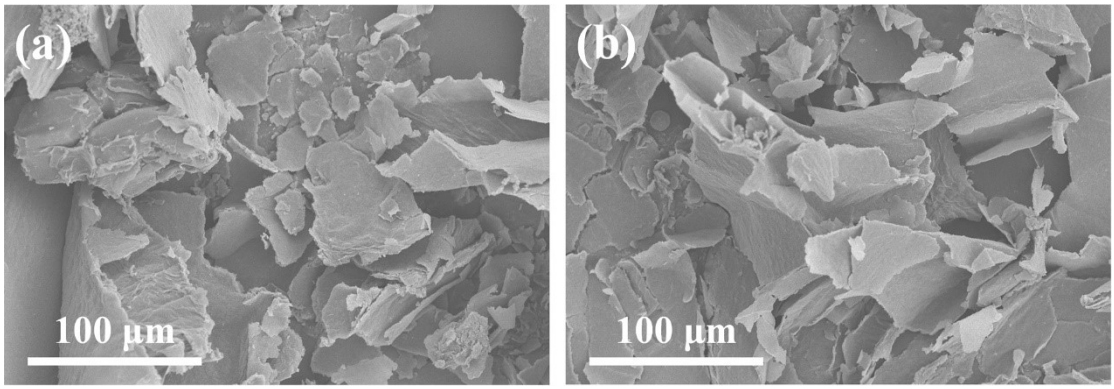

Figure S3. SEM images of the few-layer $Ti_3C_2T_x$ sheets.

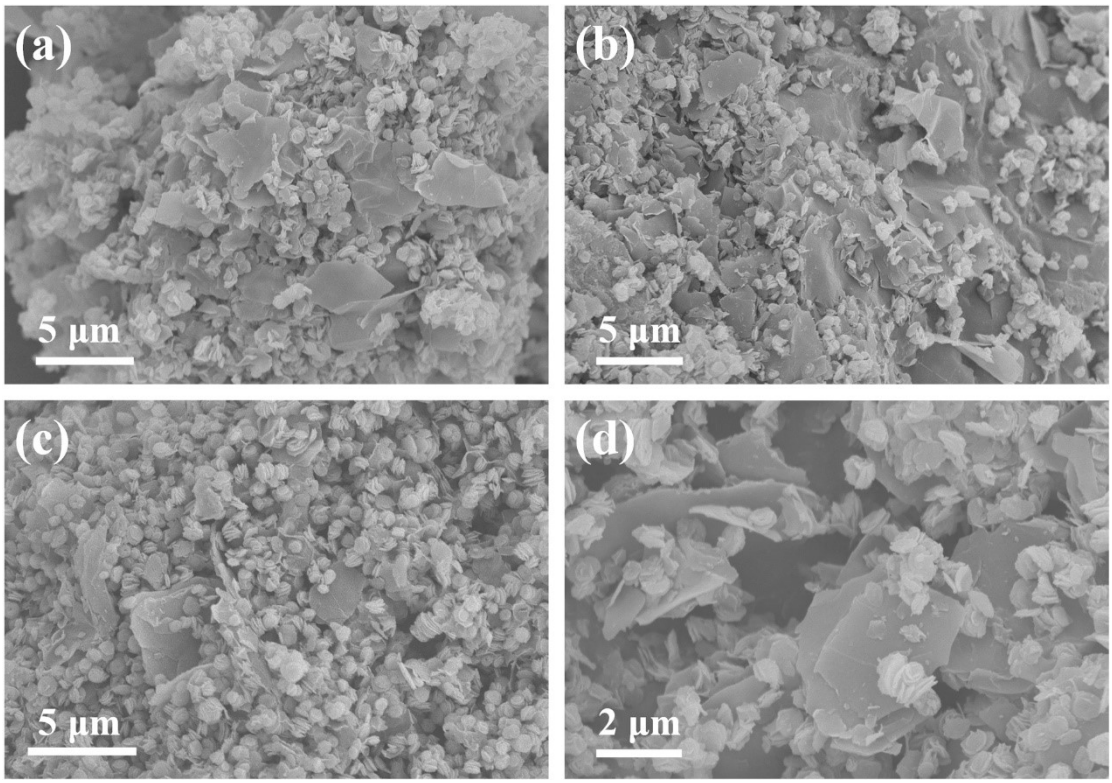

Figure S4. SEM images of $Ti_3C_2T_x/VS_2$ with different magnifications.

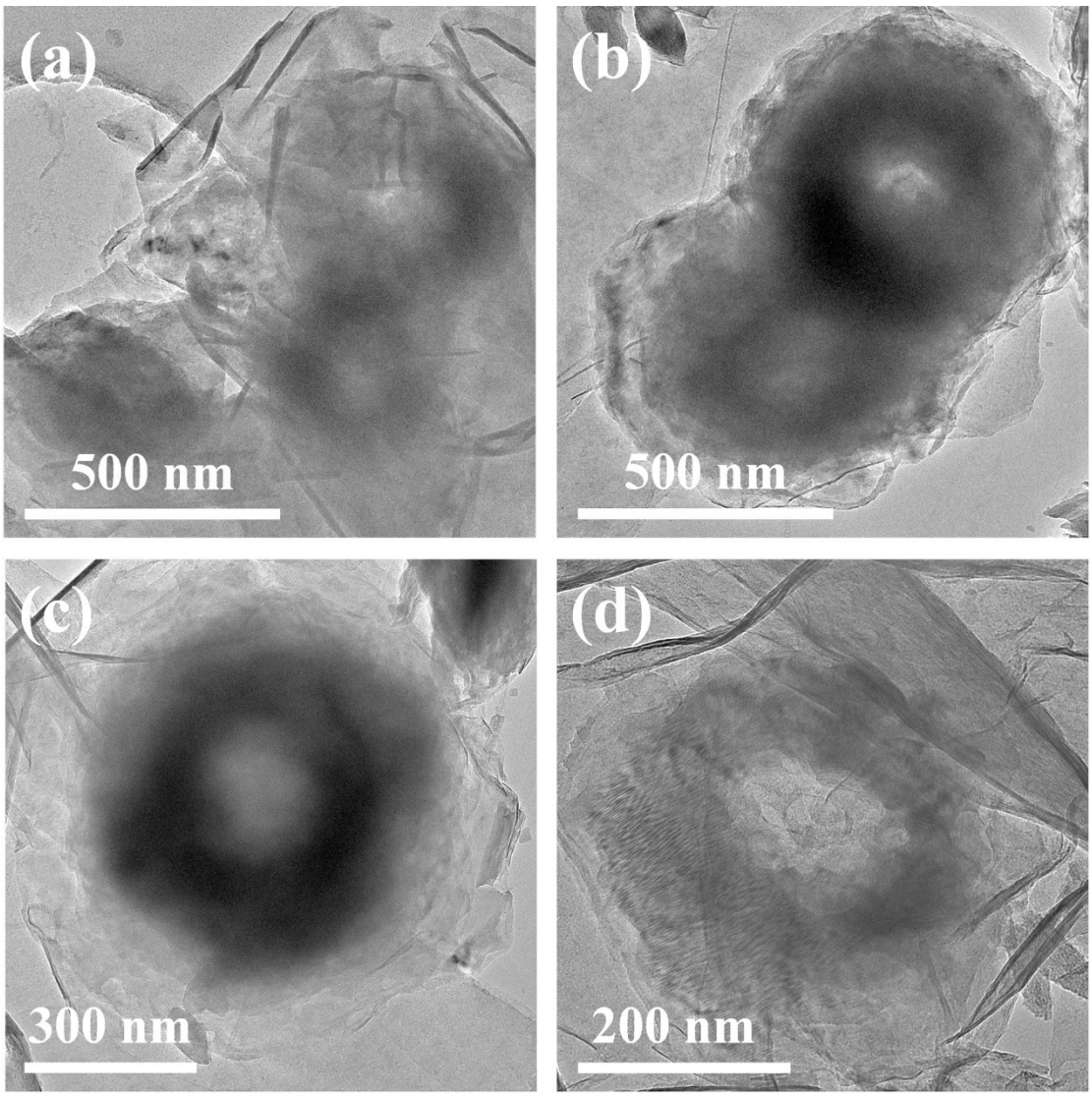

Figure S5. TEM images of $Ti_3C_2T_x/VS_2$.

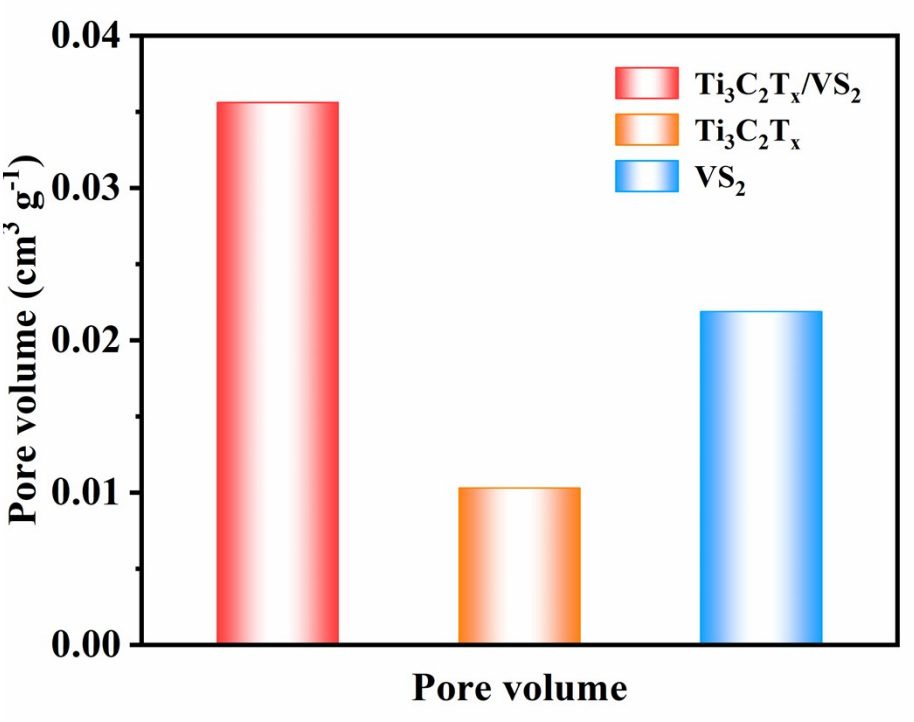

Figure S6. The pore volumes of $Ti_3C_2T_x/VS_2$, $Ti_3C_2T_x$, and VS_2.

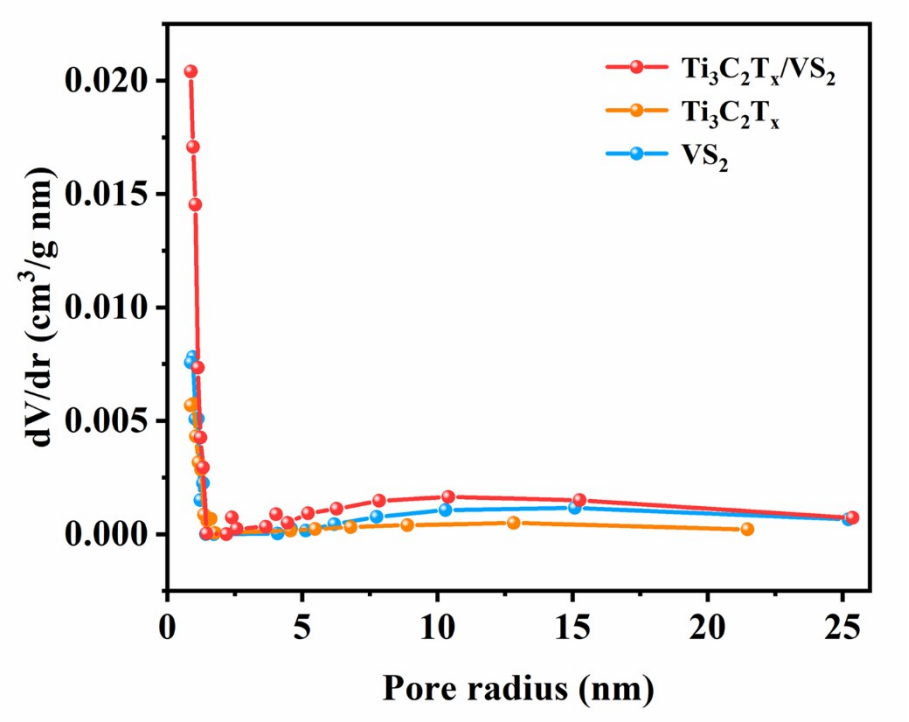

Figure S7. The pore size distribution of $Ti_3C_2T_x/VS_2$, $Ti_3C_2T_x$, and VS_2.

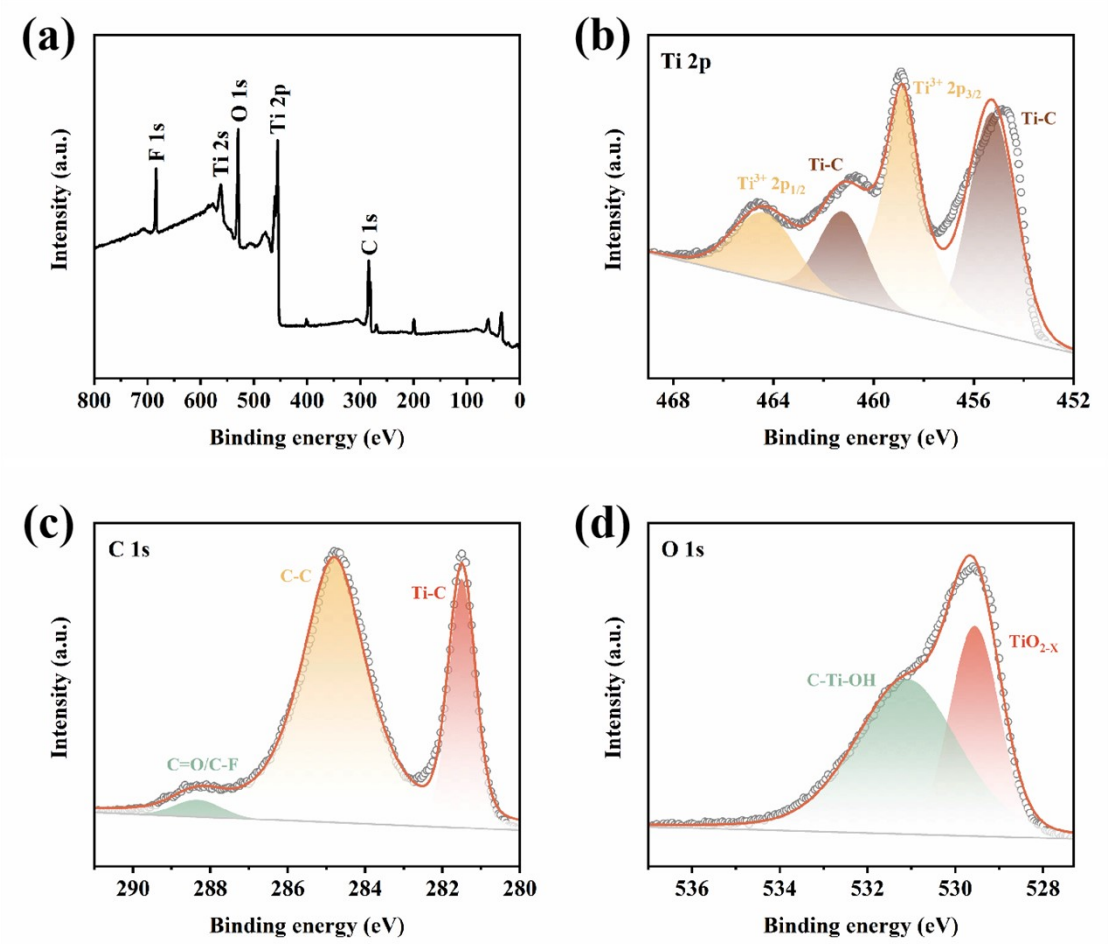

Figure S8. (a-d) XPS spectra of $Ti_3C_2T_x$: (a) survey, (b) Ti 2p, (c) C 1s, and (d) O 1s.

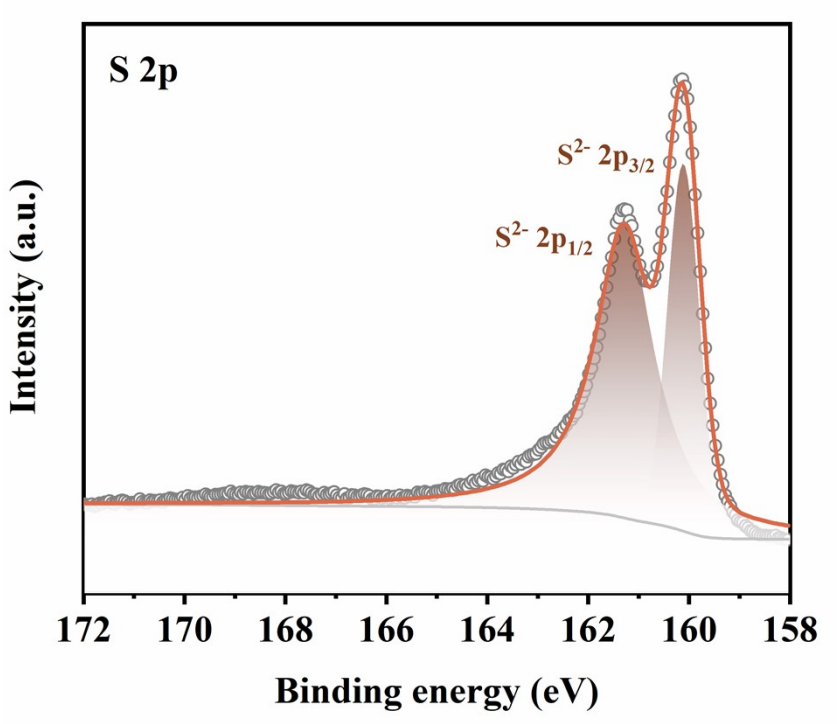

Figure S9. XPS spectrum of VS_2: S 2p.

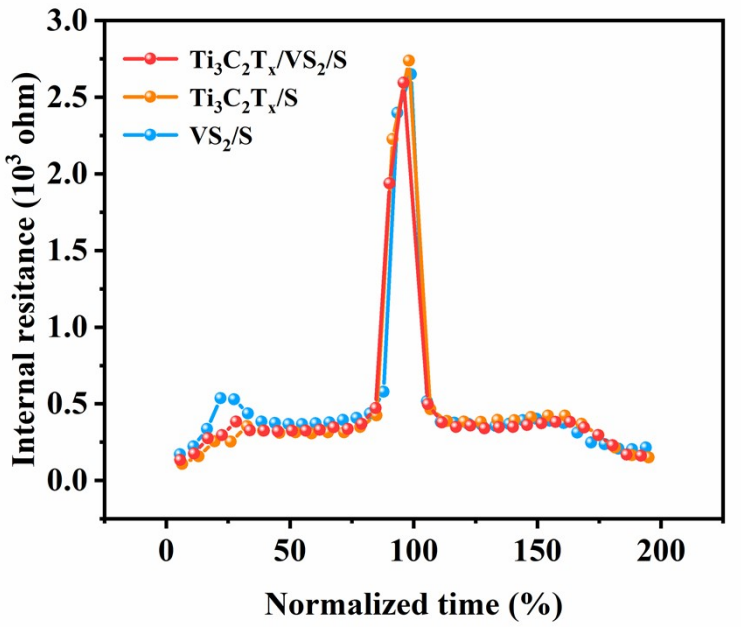

Figure S10. The corresponding internal resistances of $Ti_3C_2T_x/VS_2/S$, $Ti_3C_2T_x/S$, and VS_2/S during the discharging and charging process.

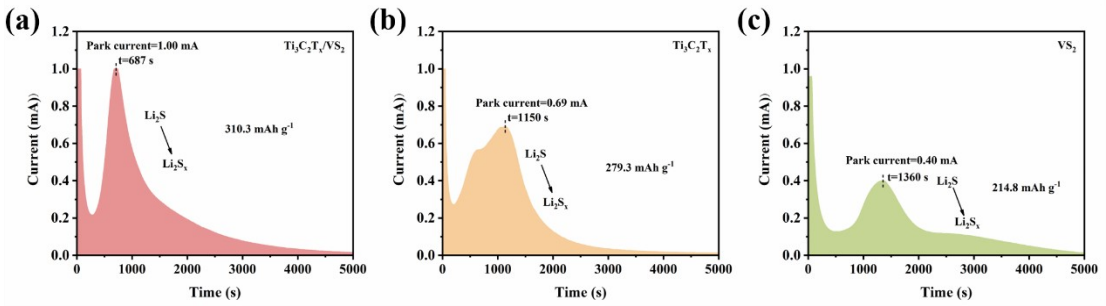

Figure S11. Li_2S dissolution profiles of $Ti_3C_2T_x/VS_2$, $Ti_3C_2T_x$, and VS_2.

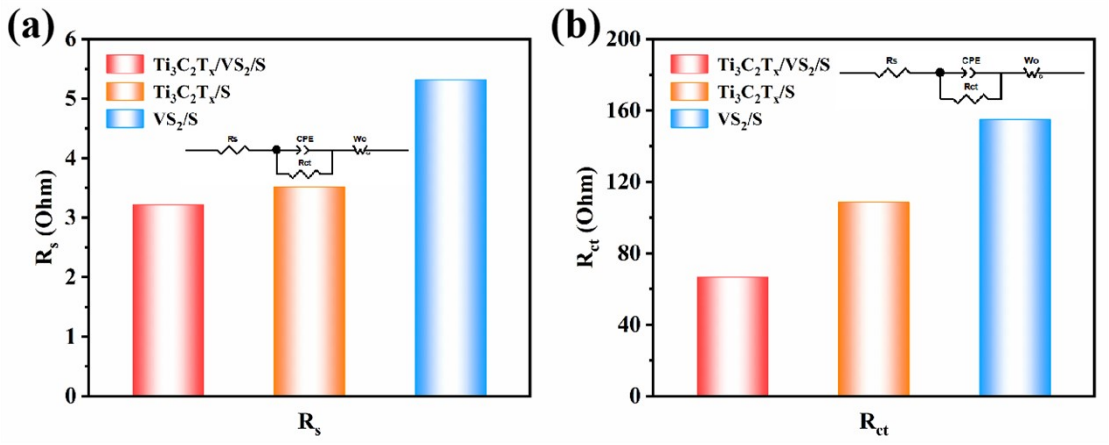

Figure S12. (a) Fitted R_s and (b) R_{ct} values for $Ti_3C_2T_x/VS_2$, $Ti_3C_2T_x$, and VS_2.

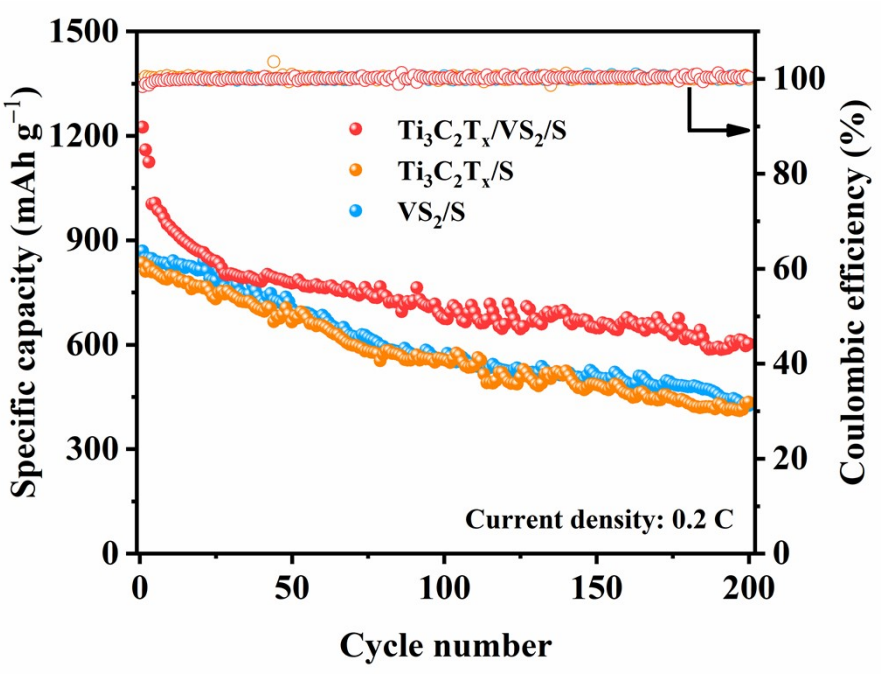

Figure S13. Cycling performance of the cells at 0.2 C.

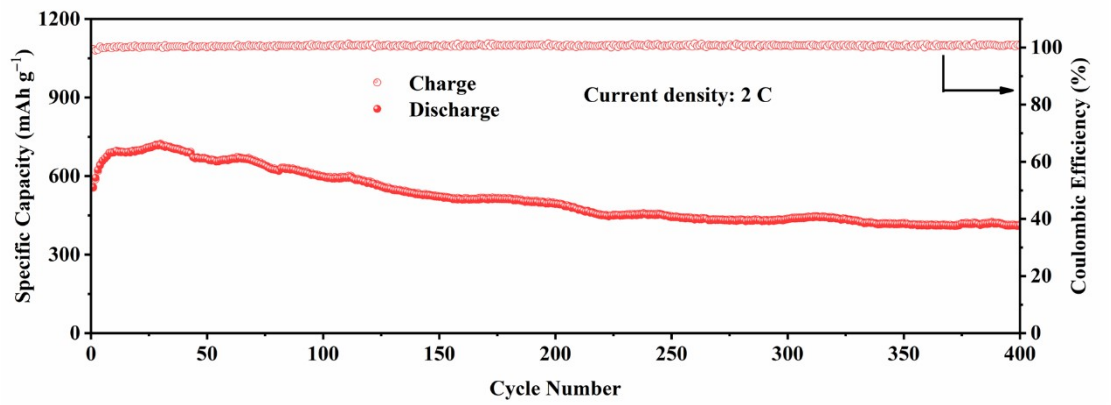

Figure S14. Cycling performance of the $Ti_3C_2T_x/VS_2/S$ at 2 C.

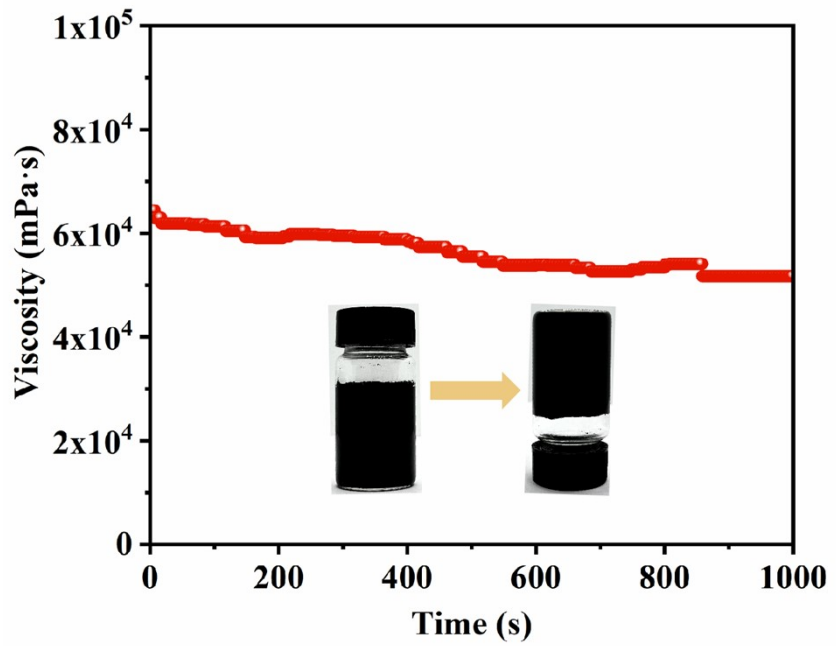

Figure S15. The viscosity of the printing slurry.

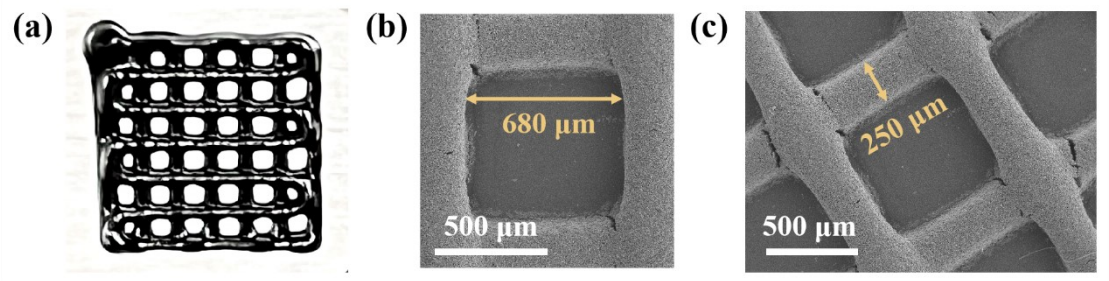

Figure S16. (a) Diagram of the 3D printed grid structure. (b-c) SEM image of the grid structure.

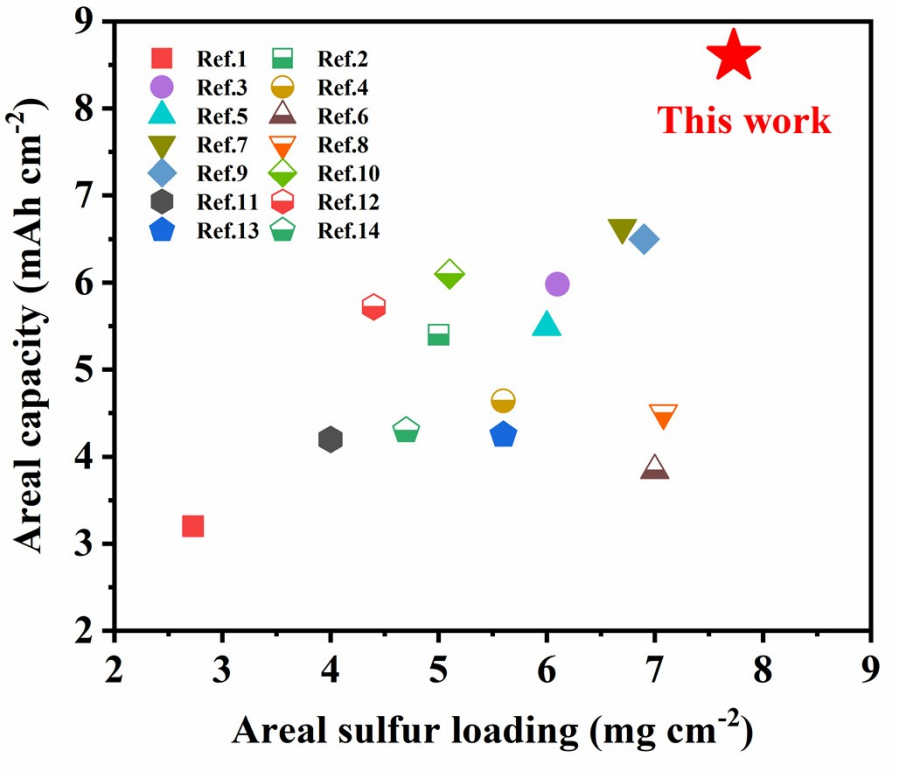

Figure S17. Comparison of area capacity of $Ti_3C_2T_x/VS_2/S$ positive electrode with other electrodes. [1-14]

References

1. W. Xi, J. Zhang, Y. Zhang, R. Wang, Y. Gong, B. He, H. Wang and J. Jin, *J. Mater. Chem. A*, 2023, **11**, 7679-7689.
2. S. Wu, W. Wang, J. Shan, X. Wang, D. Lu, J. Zhu, Z. Liu, L. Yue and Y. Li, *Energy Storage Mater.*, 2022, **49**, 153-163.
3. B. Wang, R. Fang, K. Chen, S. Huang, R. Niu, Z. Yu, G. E. P. O'Connell, H. Jin, Q. Lin, J. Liang, J. M. Cairney and D. W. Wang, *Small*, 2024, **20**, 2310801.
4. J. Lei, X. X. Fan, T. Liu, P. Xu, Q. Hou, K. Li, R. M. Yuan, M. S. Zheng, Q. F. Dong and J. J. Chen, *Nat. Commun.*, 2022, **13**, 202.
5. X. Y. Li, S. Feng, M. Zhao, C. X. Zhao, X. Chen, B. Q. Li, J. Q. Huang and Q. Zhang, *Angew. Chem. Int. Ed.*, 2022, **61**, e202114671.
6. W. Hou, P. Feng, X. Guo, Z. Wang, Z. Bai, Y. Bai, G. Wang and K. Sun, *Adv. Mater.*, 2022, **34**, e2202222.
7. D. Yang, Z. Liang, P. Tang, C. Zhang, M. Tang, Q. Li, J. J. Biendicho, J. Li, M. Heggen, R. E. Dunin-Borkowski, M. Xu, J. Llorca, J. Arbiol, J. R. Morante, S. L. Chou and A. Cabot, *Adv. Mater.*, 2022, **34**, e2108835.
8. X. Li, Q. Guan, Z. Zhuang, Y. Zhang, Y. Lin, J. Wang, C. Shen, H. Lin, Y. Wang, L. Zhan and L. Ling, *ACS Nano*, 2023, **17**, 1653-1662.
9. M. Wang, Y. Song, Z. Sun, Y. Shao, C. Wei, Z. Xia, Z. Tian, Z. Liu and J. Sun, *ACS Nano*, 2019, **13**, 13235-13243.
10. Y. Song, W. Zhao, L. Kong, L. Zhang, X. Zhu, Y. Shao, F. Ding, Q. Zhang, J. Sun

and Z. Liu, *Energy Environ. Sci.*, 2018, **11**, 2620-2630.

11. J. Wu, J. Chen, Y. Huang, K. Feng, J. Deng, W. Huang, Y. Wu, J. Zhong and Y. Li, *Sci. Bull.*, 2019, **64**, 1875-1880.
12. M. Wang, H. Yang, K. Shen, H. Xu, W. Wang, Z. Yang, L. Zhang, J. Chen, Y. Huang, M. Chen, D. Mitlin and X. Li, *Small Methods*, 2020, **4**, 2000353.
13. Q. Zeng, X. Li, W. Gong, S. Guo, Y. Ouyang, D. Li, Y. Xiao, C. Tan, L. Xie, H. Lu, Q. Zhang and S. Huang, *Adv. Energy Mater.*, 2022, **12**, 2104074.
14. C. Li, W. Ge, S. Qi, L. Zhu, R. Huang, M. Zhao, Y. Qian and L. Xu, *Adv. Energy Mater.*, 2022, **12**, 2103915.